Potential formulation of sleep dynamics

A. J. K. Phillips[1,2,*] and P. A. Robinson[1,2,3]
[1]*School of Physics, University of Sydney, New South Wales 2006, Australia*
[2]*Brain Dynamics Center, Westmead Millenium Institute, Westmead Hospital and Western Clinical School, University of Sydney, Westmead, New South Wales 2145, Australia*
[3]*Faculty of Medicine, University of Sydney, New South Wales 2006, Australia*
(Received 16 December 2008; published 24 February 2009)

A physiologically based model of the mechanisms that control the human sleep-wake cycle is formulated in terms of an equivalent nonconservative mechanical potential. The potential is analytically simplified and reduced to a quartic two-well potential, matching the bifurcation structure of the original model. This yields a dynamics-based model that is analytically simpler and has fewer parameters than the original model, allowing easier fitting to experimental data. This model is first demonstrated to semiquantitatively match the dynamics of the physiologically based model from which it is derived, and is then fitted directly to a set of experimentally derived criteria. These criteria place rigorous constraints on the parameter values, and within these constraints the model is shown to reproduce normal sleep-wake dynamics and recovery from sleep deprivation. Furthermore, this approach enables insights into the dynamics by direct analogies to phenomena in well studied mechanical systems. These include the relation between friction in the mechanical system and the timecourse of neurotransmitter action, and the possible relation between stochastic resonance and napping behavior. The model derived here also serves as a platform for future investigations of sleep-wake phenomena from a dynamical perspective.

DOI: 10.1103/PhysRevE.79.021913 PACS number(s): 87.19.L−, 87.10.−e, 87.18.Vf

I. INTRODUCTION

The dynamics of the human sleep-wake cycle are understood to be the result of drives to a system of brainstem nuclei that control arousal [1–3]. Advances in knowledge of the physiology have revealed enough of the underlying mechanisms to enable several physiologically based models of the system to be developed [4–6]. These models are able to relate dynamics directly to physiology, including the underlying causes of certain pathologies [4]. However, as more details of the physiology are included, the models become less analytically tractable and more difficult to fit to experimental data. Furthermore, the physiological mechanisms underlying certain phenomena, such as the ultradian rhythm between rapid eye movement (REM) and non-REM (NREM) sleep [7], are not yet properly understood. Only the model of Phillips and Robinson, which purposely left aside the question of what causes the ultradian rhythm, has had all its parameters rigorously constrained [4,8]. Hence, there is a need for dynamics-based models, which are ultimately still compatible with the physiological interactions underpinning them, but analytically simpler and applicable to phenomena for which the physiology is as yet still unclear.

At the core of human sleep-wake dynamics is the sleep-wake switch [1]. Mutual inhibition between wake-promoting and sleep-promoting nuclei gives rise to a "flip-flop" switch, with each group indirectly reinforcing its own firing. Only one group can be active at a time, with rapid transitions between states [1,3]. Transitions are caused by changes in drives to the system, including the approximately 24 h periodic circadian drive [9], and the homoestatic drive to sleep, which increases during wake and decreases during sleep [10]. However, our understanding of the physiology is still incomplete, and ultimately, modeling of the systems involved from a dynamical perspective may help to infer the underlying physiology.

In this paper we reframe the physiologically based model of Phillips and Robinson [4] as a mechanical system by constructing an equivalent nonconservative potential [11], providing a starting point for dynamics-based modeling. This potential is then simplified analytically, and reduced to a quartic two-well potential with the same bifurcation structure as the original model. This approach is admissible for the model chosen, since it consists of two first order differential equations, with a slowly varying drive. Variations in the drive serve to distort the two-well potential, resulting in movements between the wells that represent sleep and wake. The simplified model then serves as a model of sleep-wake dynamics in its own right—one that is more readily fitted to data and that can be interpreted from the perspective of mechanical systems.

In Sec. II we briefly describe the Phillips-Robinson model and its relation to the underlying physiology. We then derive a potential formulation of the model in Sec. III, and make analytic simplifications to its functional form. The form of nonconservative forces in the model are is considered and related to the underlying physiology. Correspondences between the original model and the simplified quartic potential are then presented in Sec. IV for normal sleep-wake behavior. The quartic potential model is then fitted to experimentally derived criteria, yielding a set of rigorous constraints on its parameters in Sec. V. The model is then shown to realistically reproduce recovery from sleep deprivation. Other phenomena, including avenues into chaotic behavior and stochastic resonance are covered in Sec. VI. Finally, the results

*ajp@physics.usyd.edu.au

and future avenues for application of this work are discussed in Sec. VII.

II. THE PHILLIPS-ROBINSON MODEL

The overall arousal state of the brain is regulated by a series of brainstem nuclei, collectively termed the ascending arousal system (AAS). These nuclei project diffusely to the cortex and thalamus, and can be classified as monoaminergic (MA) or acetylcholine-related (ACh) depending on their neuromodulatory properties and firing patterns [2]. The AAS is in turn modulated by circadian and homeostatic drives, which are relayed via the ventrolateral preoptic area (VLPO). The circadian drive originates in the suprachiasmatic nucleus (SCN), which generates a self-sustaining oscillation of approximately 24 h period that is entrained by light. The homeostatic drive is a drive to sleep that increases with time spent awake, and is believed to be due to the accumulation of metabolic by-products, such as adenosine [12].

The Phillips-Robinson model [4] is a neuronal population model in which average properties are assigned to populations of neurons. Each population has a mean cell body voltage V_j, and mean firing rate Q_j, where $j=m,v$ for the MA and VLPO groups, respectively. The firing rate is a sigmoidal function of the voltage

$$Q(V_j) = \frac{Q_{\max}}{1+\exp[(\theta - V_j)/\sigma']}, \tag{1}$$

where $Q_{\max}$ is the maximum possible rate; θ is the mean firing threshold relative to resting and $\sigma'\pi/\sqrt{3}$ is its standard deviation [13], determining the sigmoid width. Physiological interactions between the populations are represented by

$$\tau_m dV_m/dt = -V_m + \nu_{mv}Q_v + A, \tag{2}$$

$$\tau_v dV_v/dt = -V_v + \nu_{vm}Q_m + D, \tag{3}$$

where τ_j is the characteristic neuromodulatory decay time, ν_{ab} represents the input strength to population a from population b, $D=\nu_{vc}C+\nu_{vh}H$ is the total sleep drive, and A includes drives of cholinergic and orexinergic origin. The MA and VLPO groups are mutually inhibitory ($\nu_{mv},\nu_{vm}<0$), as shown in Fig. 1, giving rise to flip-flop dynamics in which only one population fires rapidly at a time. These states correspond to wake (MA active, VLPO inactive) and sleep (MA inactive, VLPO active).

The circadian drive is considered here to be well entrained, and so is approximated by a 24 h periodic sinusoidal signal

$$C(t) = c_0 + \cos(\omega_\oplus t), \tag{4}$$

where $\omega_\oplus=(2\pi/24)$ h^{-1}. The homeostatic drive H follows:

$$\chi dH/dt + H = \mu Q_m, \tag{5}$$

with χ being the characteristic decay time, and μ weighting production as a linear function of Q_m, since activity of the MA group is well correlated with arousal. As shown in Fig. 2, the homeostatic drive grows during wake as somnogens accumulate, and declines during sleep as they are cleared.

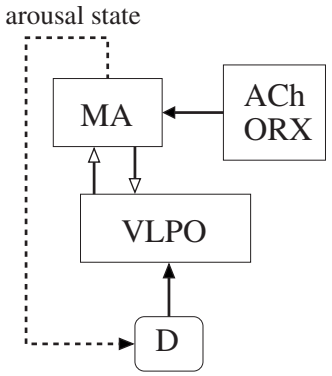

FIG. 1. Schematic of the Phillips-Robinson model of the ascending arousal system. Connections between neuronal populations are indicated by arrows, solid for excitatory, and hollow for inhibitory. The wake-active MA and the sleep-active VLPO are mutually inhibitory. The MA group also receives exitatory input for cholinergic and orexinergic sources (ACh/ORX). The VLPO is driven by $D=\nu_{vc}C+\nu_{vh}H$, and arousal state feeds back on to homeostatic production.

The parameter values used in this paper are given in Table I.

III. POTENTIAL FORMULATION

We derive a potential formulation of the Phillips-Robinson model in Secs. III A and III B. An analytic simplification to yield a quartic potential is then presented in Sec. III C, and the point about which the quartic expansion is performed is constrained in Sec. III D so as to make the dynamics of the quartic potential model closely match those of the original model. The nonconservative forces are then examined in Sec. III E, and related to the underlying physiology.

A. Construction of the potential

The normal dynamics of the model consist of slow variations within wake or sleep states, and relatively rapid ($\sim$10 min) transitions between states, as shown in Fig. 2. The drive D varies on the timescale of a day, and since

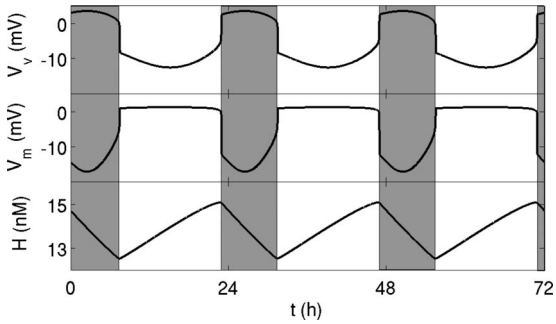

FIG. 2. Normal dynamics of the Phillips-Robinson sleep model, showing time series of (a) V_v, (b) V_m, (c) H. The dynamics are 24 h periodic, and consist of long periods of wake (low V_v, high V_m) and sleep (high V_v, low V_m), with rapid transitions between states. Sleep periods are shaded.

TABLE I. Parameter values for the Phillips-Robinson model. Constraints on these parameters are discussed in Refs. [4,8].

Parameter	Value	Unit
ν_{vc}	−2.9	mV
ν_{vh}	1.0	mV nM^{-1}
χ	45	h
μ	4.4	nM s
c_0	4.5	1
$Q_{\max}$	100	s^{-1}
θ	10	mV
σ'	3	mV
A	1.3	mV
ν_{vm}	−2.1	mV s
ν_{mv}	−1.8	mV s
τ_m	10	s
τ_v	10	s

$\chi, 1/\omega \gg \tau_m, \tau_v$, there is a natural separation of time scales. On time scales much shorter than a day, the drive can be considered slowly varying, and treated as a control parameter, reducing the system to the two first order differential equations (2) and (3). By combining these into a single second order equation, we can treat the system in terms of the dynamics of a particle in a nonconservative one-dimensional potential well. We construct this potential in terms of V_m rather than V_v as it simplifies the dynamics at the right endpoint of the potential, as discussed in Sec. III B below. Differentiating Eq. (2) with respect to time yields

$$\tau_m \frac{d^2V_m}{dt^2} = -\frac{dV_m}{dt} + \frac{\nu_{mv}Q_v}{\sigma'\left[1+\exp\left(\frac{V_v-\theta}{\sigma'}\right)\right]}\frac{dV_v}{dt}. \quad (6)$$

Rearranging Eq. (1) then yields

$$\left[1+\exp\left(\frac{V_v-\theta}{\sigma'}\right)\right]^{-1} = \frac{Q_{\max}-Q_v}{Q_{\max}} \quad (7)$$

$$= \frac{\nu_{mv}Q_{\max} - \tau_m\dot{V}_m - V_m + A}{\nu_{mv}Q_{\max}}, \quad (8)$$

upon substituting $\nu_{vm}Q_v = \tau_m V_m + V_m - A$ from Eq. (2). Inverting the sigmoid equation (1) then gives an expression for V_v in terms of V_m and $\dot{V}_m$:

$$V_v = \theta - \sigma' \ln\left(\frac{Q_{\max}-Q_v}{Q_v}\right) \quad (9)$$

$$= \theta - \sigma' \ln\left(\frac{\nu_{mv}Q_{\max} - \tau_m\dot{V}_m - V_m + A}{\tau_m\dot{V}_m + V_m - A}\right). \quad (10)$$

Substituting Eqs. (8) and (10) into Eq. (6) then yields the desired second order equation for $x \equiv V_m$:

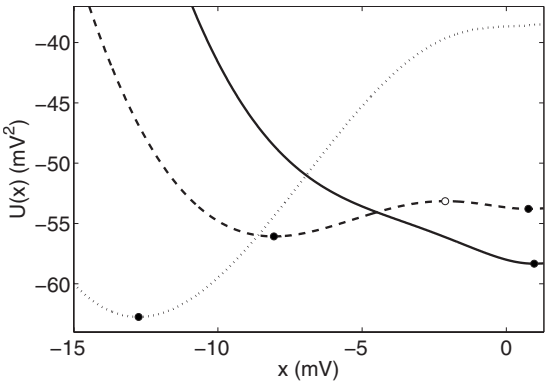

FIG. 3. The conservative potential function $U(x)$ is shown for different values of the drive D. The solid, dashed, and dotted lines correspond to $D=1.0, 1.8, 2.7$ mV, respectively. Stable steady states are indicated by filled circles and unstable steady states by unfilled circles. For $D=1.0$ mV, there is one stable state, corresponding to wake. Similarly, for $D=2.7$ mV, there is one stable state, corresponding to sleep. For $D=1.8$ mV, there are two stable steady states, corresponding to wake and sleep, and one unstable steady state. As explained in Sec. III B, the conservative potential is only defined for $x<A=1.3$ mV.

$$\tau_m\tau_v\ddot{x} = -\tau_v\dot{x} + (\nu_{mv}Q_{\max} - \tau_m\dot{x} - x + A) \times\left[\nu_{vm}S(x) + D - S^{-1}\left(\frac{\tau_m\dot{x}+x-A}{\nu_{mv}}\right)\right]\frac{\tau_m\dot{x}+x-A}{\sigma'Q_{\max}\nu_{mv}}. \quad (11)$$

This can be thought of as an equation describing the force $F=m\ddot{x}$ acting on a particle moving in one dimension, where $m=\tau_m\tau_v$ effectively plays the role of mass (but has different units). The corresponding generalized potential is

$$F(x,\dot{x}) = -\int_{x_0}^{x} -\tau_v\dot{x} + (\nu_{mv}Q_{\max} - \tau_m\dot{x} - u + A) \times\left[\nu_{vm}S(u) + D - S^{-1}\left(\frac{\tau_m\dot{x}+u-A}{\nu_{mv}}\right)\right] \times\frac{\tau_m\dot{x}+u-A}{\sigma'Q_{\max}\nu_{mv}}du. \quad (12)$$

This is a nonconservative potential [11], since it depends on the velocity $\dot{x}$. The conservative component of the generalized potential is

$$U(x) = F(x,0) = -\int_{x_0}^{x} (\nu_{mv}Q_{\max} - u + A) \times\left[\nu_{vm}S(u) + D - S^{-1}\left(\frac{u-A}{\nu_{mv}}\right)\right] \times\frac{u-A}{\sigma'Q_{\max}\nu_{mv}}du. \quad (13)$$

The conservative potential is shown in Fig. 3 for a range of values of D. As D is increased, the system goes from having one stable equilibrium (one well corresponding to wake), to two stable equilibriums and one unstable equilibrium (two

wells corresponding to wake and sleep), to having one stable equilibrium (one well corresponding to sleep).

B. Right endpoint

The behavior of the system at the right endpoint of the potential requires further explanation, since the potential becomes complex-valued for $x > A - \tau_m \dot{x}$. This region corresponds to unphysical values with $Q_v < 0$ as seen by rearranging Eq. (2) to $\nu_{vm} Q_v = \tau_m \dot{x} + x - A$, and since $\dot{x} < 0$ whenever $x > A - \tau_m \dot{x}$, it is not possible for the system to enter this region.

To obtain a satisfactory physical interpretation of the potential well, the endpoint must be treated carefully. In the limit $\tau_m \dot{x} + x \to A^-$ we use L'Hôpital's rule to find

$$\tau_v \tau_m \ddot{x} \to -\tau_v \dot{x} - \frac{\nu_{mv}}{\sigma'} V_v Q_v = -\tau_v \dot{x}, \tag{14}$$

implying that the conservative potential flattens out at the right endpoint, since there are no velocity independent forces acting. The implication is therefore that the particle is constrained within the allowed region by nonconservative forces. We note that by constructing our potential in terms of V_m rather than V_v, the position of this endpoint is independent of D, which simplifies the above analysis.

C. Quartic expansion

The exact analytic solution of the integral in Eq. (12) is cumbersome, since it includes a polylogarithmic term from integration of the sigmoid term. We are therefore interested in finding simplifying analytic approximations. During a normal sleep-wake cycle of the sleep model, we find typical firing rates of less than about $10\ \mathrm{s}^{-1}$ at all times, in agreement with physiological data. Thus, it is reasonable to assume $Q_v \ll Q_{\max}$, which simplifies Eq. (10) to

$$V_v \simeq \theta + \sigma' \ln(Q_v/Q_{\max}) = \theta + \sigma' \ln\left(\frac{\tau_m \dot{x} + x - A}{Q_{\max} \nu_{mv}}\right). \tag{15}$$

Similarly, assuming $Q_m \ll Q_{\max}$ simplifies Eq. (1) to

$$Q_m(x) \simeq Q_{\max} \exp\left(\frac{x - \theta}{\sigma'}\right). \tag{16}$$

Using these approximations in Eq. (13) gives the simplified form of the conservative potential

$$U(x) = -\frac{1}{\sigma'} \int_{x_o}^{x} (u - A) \left[\nu_{vm} Q_{\max} \exp\left(\frac{u - \theta}{\sigma'}\right) + D - \theta - \sigma' \ln\left(\frac{u - A}{Q_{\max} \nu_{mv}}\right) \right] du, \tag{17}$$

$$= b + \nu_{vm} Q_{\max} (A + \sigma' - x) \exp\left(\frac{x - \theta}{\sigma'}\right) + \frac{1}{2\sigma'} (x - A)^2 \left[\theta - D - \frac{\sigma'}{2} + \sigma' \ln\left(\frac{x - A}{\nu_{mv} Q_{\max}}\right) \right], \tag{18}$$

where b is a constant of integration.

Since $U(x)$ is a two-well potential, as seen in Fig. 3, we are motivated to derive a quartic approximation. We achieve this by Taylor expanding about a point $x = x_0$ (the procedure by which x_0 is chosen is described below) to fourth order to yield the following series:

$$U = a_1 (x - x_0) + a_2 (x - x_0)^2 + a_3 (x - x_0)^3 + a_4 (x - x_0)^4 + O[(x - x_0)^5], \tag{19}$$

where we have set the zeroth-order term of the potential to zero without loss of generality, and

$$a_1 = \frac{A - x_0}{\sigma'} \left[D - \theta + \nu_{vm} Q_{\max} \exp\left(\frac{x_0 - \theta}{\sigma'}\right) - \sigma' \ln\left(\frac{x_0 - A}{\nu_{mv} Q_{\max}}\right) \right], \tag{20}$$

$$a_2 = \frac{1}{2\sigma'^2} \left[\nu_{vm} Q_{\max} (A - x_0 - \sigma') \exp\left(\frac{x_0 - \theta}{\sigma'}\right) + \sigma' \left(\sigma' + \theta - D + \sigma' \ln\left\{ \frac{x_0 - A}{\nu_{mv} Q_{\max}} \right\} \right) \right], \tag{21}$$

$$a_3 = \frac{1}{6} \left[\frac{\nu_{vm} Q_{\max} (A - x_0 - 2\sigma')}{\sigma'^3} \exp\left(\frac{x_0 - \theta}{\sigma'}\right) - \frac{1}{A - x_0} \right], \tag{22}$$

$$a_4 = \frac{1}{24} \left[\frac{\nu_{vm} Q_{\max} (A - x_0 - 3\sigma')}{\sigma'^4} \exp\left(\frac{x_0 - \theta}{\sigma'}\right) - \frac{1}{(A - x_0)^2} \right]. \tag{23}$$

The first and second order terms in $(x - x_0)$ are found to depend linearly on the drive D, whereas the third and fourth order terms are independent of D. We can therefore also represent the potential in the form

$$U = f(x; x_0) + D g(x; x_0), \tag{24}$$

where

$$f(x; x_0) = \left[a_1 - \frac{D(A - x_0)}{\sigma'} \right] (x - x_0) + \left(a_2 + \frac{D}{2\sigma'} \right) (x - x_0)^2 + a_3 (x - x_0)^3 + a_4 (x - x_0)^4 \tag{25}$$

and

$$g(x; x_0) = \frac{A - x_0}{\sigma'} (x - x_0) - \frac{1}{2\sigma'} (x - x_0)^2. \tag{26}$$

The functions f and g are plotted in Fig. 4 for various values of x_0. The function f is a quartic with a positive fourth order

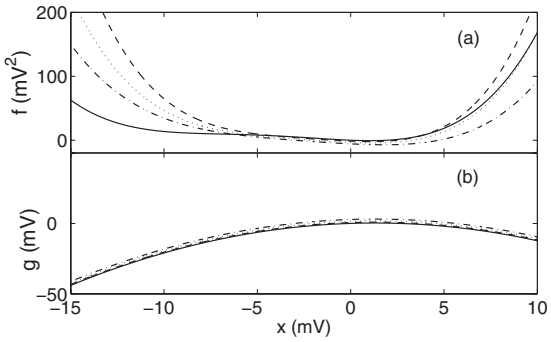

FIG. 4. Plots of (a) the drive independent component of the potential $f(x;x_0)$ and (b) the linear coefficient of the drive-dependent component of the potential $g(x;x_0)$. Functions are shown for $x_0=0$ mV (solid), −1 mV (dashed), −2 mV (dotted), −3 mV (dash-dotted).

coefficient, while g is a quadratic with negative second order coefficient, with both functions having their extremums at $x \simeq 1$ mV (the exact positions depending on x_0). Thus, for negative values of D, the sum in Eq. (24) results in a single minimum at $x \simeq 1$ mV, corresponding to wake. For large positive values of D, the sum results in no minimum there, and instead a minimum at negative x, corresponding to sleep, as per Fig. 3. For intermediate values of D, the system is bistable, with both wake and sleep states present.

To accurately represent the potential, it is necessary to choose the value of x_0 appropriately, in particular so as to have the right curvature, and also to be consistent with behavior at the right endpoint discussed in Sec. III B. In Fig. 5 we plot the values of the coefficients of the quartic potential as a function of the value of x_0. We find that if the curvature of the quartic is to be correct—i.e., to ensure the fourth order term has a positive coefficient—x_0 must satisfy -6.2 mV $< x_0 < 0.2$ mV. Furthermore, x_0 must be sufficiently close to the right endpoint, so that the particle does not move into the unphysical region $x > A - \tau_m \dot{x}$, an issue considered in more detail in Sec. III D below.

D. Expansion point

The behavior of the simplified model expressed in Eq. (34) depends sensitively on the value of x_0 chosen. Steady state solutions to Eq. (34) correspond to

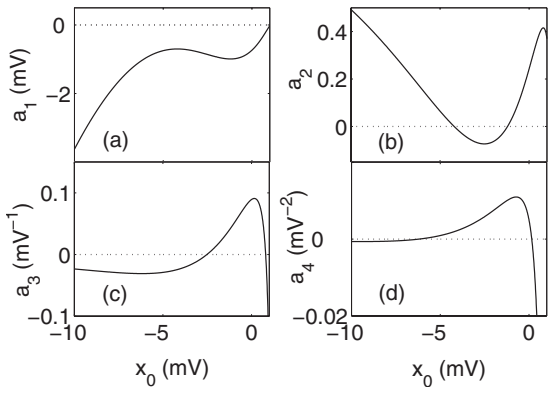

FIG. 5. The coefficients of the quartic conservative potential of Eq. (19), as functions of x_0, setting $D=1$ mV. (a) a_1, (b) a_2, (c) a_3, (d) a_4.

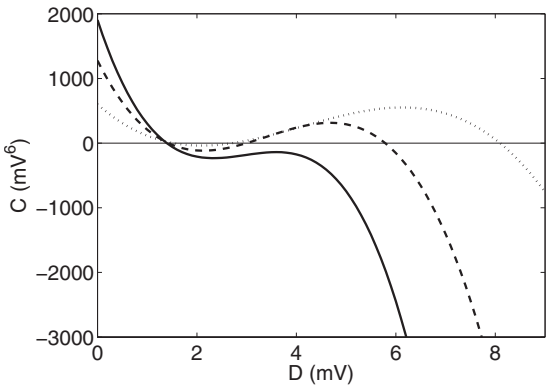

FIG. 6. Plot of the function $C(D)$, which is positive where the system has one steady state solution and negative where it has three. The function is shown for $x_0=-2.4$ mV (solid), −2.0 mV (dashed), −1.0 mV (dotted).

$$4a_4(x-x_0)^3 + 3a_3(x-x_0)^2 + 2a_2(x-x_0) + a_1 = 0, \quad (27)$$

and since all the coefficients of the cubic are real, the number of real solutions is given by the sign of $C=Q^3+R^2$, with

$$Q = (8a_2a_4 - 3a_3^2)/(48a_4^2) \quad (28)$$

and

$$R = (4a_2a_3a_4 - 8a_1a_4^2 - a_3^3)(64a_4^3). \quad (29)$$

For $C>0$, there is one real solution, and for $C<0$ there are three real solutions. As shown in Fig. 6, C is a cubic function of D, and changes to the value of x_0 change the points of intersection with the D axis. For $x_0<-2.3$ mV, there is only one intersection, implying a single steady state solution for low values of D, and three steady state solutions (two stable, one unstable) for high values of D. This would not be a good representation of the dynamics of the full model, which undergoes transitions from one steady state solution (corresponding to wake), to three (wake, sleep, and one unstable), and back to one (corresponding to sleep) as D is increased. Therefore, we are restricted to -2.3 mV $< x_0 < 0.2$ mV.

For $x_0>-2.3$ mV, the function $C(D)$ intersects $C=0$ three times, passing through four zones as D is increased: (i) one steady state solution (wake), (ii) three solutions (wake, sleep, and an unstable state), (iii) one solution (sleep), then (iv) three solutions (wake, sleep, and an unstable state). The reason for the existence of the fourth region is the dependence of a_2 on D. For large values of D, the quadratic term in the quartic potential becomes large and negative, resulting in the reemergence of a two-well potential. However, since this fourth region is only accessible at unrealistically high levels of D, it does not pose a problem when it comes to reproducing normal model dynamics.

Varying x_0 changes the width of the bistable region [i.e., region (ii) above], and this is illustrated in Fig. 7, along with the width of the bistable zone of the full model. The width is found to be greater for the simplified model than for the full model, but we find that it lies within 30% of the full model's

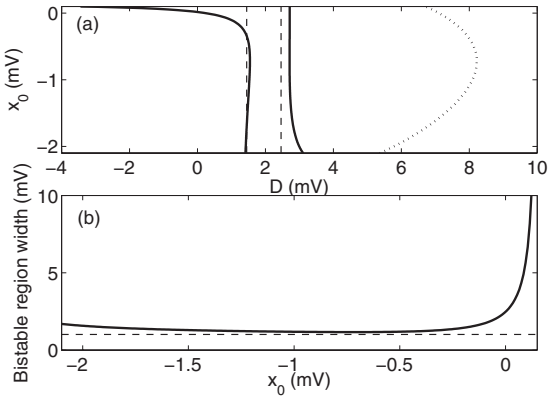

FIG. 7. (a) Boundaries of the regions (i)–(iv) described in Sec. III D, as a function of x_0. The boundaries of the bistable region (ii) are illustrated by thick solid lines for the quartic potential, with region (i) lying to the left of the leftmost line. For comparison, the width of the bistable region for the full model is shown with dashed lines. The boundary between regions (iii) and (iv) is also shown as a dotted line. (b) Width of the bistable region (ii) as a function of x_0, for the quartic potential (solid line), and full model (dashed line).

value for $-1.5\ \mathrm{mV} < x_0 < -0.3\ \mathrm{mV}$. The behavior of the quartic potential model is investigated in Sec. IV below for values of x_0 within this range.

E. Friction

The conversion to a mechanical model allows us to reinterpret the dynamics in terms of well studied phenomena in mechanical systems. We now show that the nonconservative forces in this system are approximately frictional, and show how they are related to the underlying physiology. Taking the partial derivative of Eq. (11) with respect to $\dot{x}$ yields

$$\frac{\partial(\tau_m\tau_v\ddot{x})}{\partial\dot{x}} = -(\tau_m+\tau_v) + \tau_v\frac{(\nu_{mv}Q_v + A - V_m)(\nu_{vm}Q_{\max} - 2\tau_v\dot{x} - 2x + 2D)}{\sigma' Q_{\max}\nu_{vm}}. \tag{30}$$

Using Eqs. (2) and (3) this simplifies to

$$\frac{\partial(\tau_m\tau_v\ddot{x})}{\partial\dot{x}} = -(\tau_m+\tau_v) + \frac{\tau_v\tau_m\dot{V}_m(Q_{\max}-2Q_m)}{\sigma' Q_{\max}}, \tag{31}$$

which can be further simplified under the assumption $Q_m \ll Q_{\max}$ to

$$\frac{\partial(\tau_m\tau_v\ddot{x})}{\partial\dot{x}} = -(\tau_m+\tau_v) + \frac{\tau_v\tau_m\dot{V}_m}{\sigma'}. \tag{32}$$

In transitions between the stable states of wake and sleep, the mean cell body voltage V_m changes by $\lesssim 10$ mV in a time of $\gtrsim 2$ min, corresponding to $\dot{V}_m \lesssim 0.1\ \mathrm{mV\ s^{-1}}$. The second term is thus $\lesssim 3$ s, whereas $\tau_m+\tau_v \simeq 20$ s. The first term will thus dominate, yielding

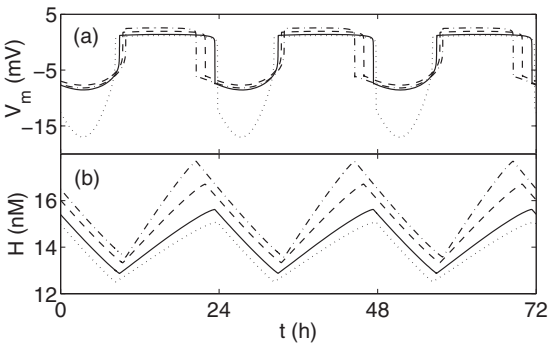

FIG. 8. Dynamics of the model, showing (a) V_m and (b) H. The quartic potential dynamics are shown for $x_0 = -0.3$ mV (solid), -0.9 mV (dashed), -1.5 mV (dash-dotted), and for the full model (dotted).

$$\frac{\partial(\tau_m\tau_v\ddot{x})}{\partial\dot{x}} \simeq -(\tau_m+\tau_v). \tag{33}$$

This implies that the dissipative force is approximately frictional for normal model dynamics. Hence, the overall dynamics can be approximated by the simpler form

$$m\ddot{x} = -a_1 - 2a_2(x-x_0) - 3a_3(x-x_0)^2 - 4a_4(x-x_0)^3 - \kappa\dot{x}, \tag{34}$$

where $m=\tau_m\tau_v$ is the effective mass of the particle and $\kappa = \tau_m+\tau_v$ is the effective coefficient of friction. This mechanical analog can be interpreted physiologically as dictating the time taken for the model to move between wake and sleep states. Furthermore, this perspective reveals that if κ is too small, the potential model exhibits damped oscillations about the steady state following transitions; i.e., ringing in the system.

IV. COMPARISON OF SIMPLIFIED AND FULL MODELS

Having now constrained the range of reasonable values for x_0, we compare the normal dynamics of the simplified model with those of the full Phillips-Robinson model, exploring the sensitivity to x_0. We find that the normal dynamics of the two models are qualitatively similar across the whole range $-1.5\ \mathrm{mV} < x_0 < -0.3\ \mathrm{mV}$, with most time being spent in either the wake state or the sleep state, and with rapid transitions between states, as seen in Fig. 8. However, for lower values of x_0, the simplified model does not provide as good a fit to the waking voltage and firing rate, as shown in Fig. 9, nor does it fit the times of transition between wake and sleep as well. The dynamics of the full model are best fitted by values of x_0 near the upper end of the range. The VLPO firing rates are then not fitted as well, due to x_0 being further from the sleep state, and therefore the quartic expansion is not as good a representation of the potential there. However, due to the firing rate being a sigmoidal function of x, this makes no appreciable difference to the MA firing rates during sleep, and therefore does not affect the sleep-wake dynamics significantly, which are dictated by the firing rate of the MA group.

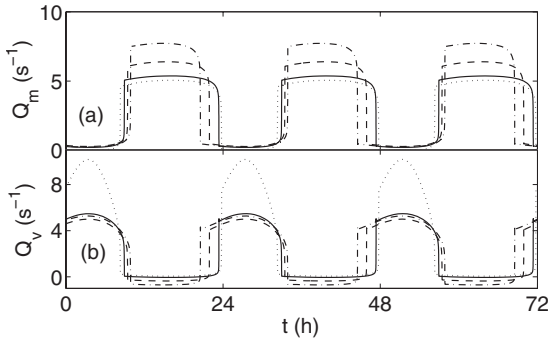

FIG. 9. Dynamics of the model, showing (a) Q_m and (b) Q_v. The quartic potential dynamics are shown for $x_0=-0.3$ mV (solid), −0.9 mV (dashed), −1.5 mV (dash-dotted), and for the full model (dotted).

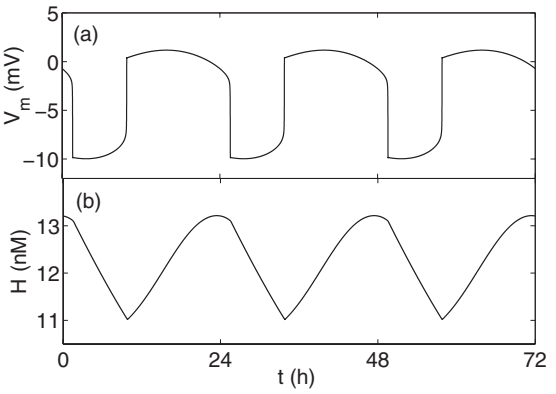

FIG. 10. Dynamics of the quartic model with nominal parameter values, showing (a) V_m and (b) H.

V. MODEL FITTING

We now use the quartic potential as a model of sleep-wake dynamics in its own right by constraining its parameters directly, using experimentally derived criteria, rather than trying to match it to the model it was derived from. This is indeed a more appropriate way of constraining the model to reproduce dynamics that simulate actual data. In this section, we use the form

$$\tau_v \tau_m \ddot{x} = k_3(x-x_0)^3 + k_2(x-x_0)^2 + k_1(x-x_0) + k_0 + k_d D - (\tau_v + \tau_m)\dot{x}, \tag{35}$$

where k_3, k_2, k_1, k_0, and k_d are constants to be constrained, and we use $x_0=-0.3$ mV based on the results in Sec. IV. To further simplify the model, we have dropped the drive-dependent linear term $D(x-x_0)$, since the lower order term k_dD is already sufficient to generate normal dynamics.

We explore parameter space to find any regions that satisfy the following physiologically based criteria: (i) normal sleep duration in the range 7 to 10 h, (ii) hysteresis loop crossing time in the range 1 to 3 h as per previous work [4], (iii) Q_m in the range 3 to 5.5 s^{-1} during wake, and (iv) Q_m in the range 0 to 0.5 s^{-1} during sleep, to match physiologically realistic firing rates [4,8]. The parameters that satisfy all of these criteria are found to lie in the ranges $k_3 < -0.006$ mV^{-2}, $k_2 < 0$ mV^{-1}, $k_1 < -0.15$, $k_0 > 0.1$ mV, $k_d < -0.1$. We choose a nominal set of parameters from near the center of the acceptable region $k_3=-0.03$ mV^{-2}, $k_2=-0.4$ mV^{-1}, $k_1=-1.2$, $k_0=0.7$ mV, $k_d=-0.2$, and use $x_0=-0.3$ mV, consistent with Sec. IV. The model dynamics for these parameter values are shown in Fig. 10, with the dynamics satisfying all constraints. The model output also semiquantitatively matches the original model, despite being constrained separately.

As an additional test of the dynamics of the simplified quartic potential model, we now apply sleep deprivation. To model sleep deprivation, we hold the model in the waking state by setting $\ddot{x}=\dot{x}=0$ in the simplified model. This simulates the effect of a wake-promoting drive that is just sufficient to maintain the model in wake. As initial values, we set $x=0.5$ mV, corresponding to a typical waking value, and $H=13.2$ nM, corresponding to the normal level of H at sleep onset. As seen in Fig. 11, the homeostatic drive continuously rises during the enforced waking state, its dynamics still being dictated by Eq. (5). By releasing the enforced waking conditions, the models then undergo recovery sleep, returning to normal dynamics over the course of two to three nights, and sleeping an extra 6.4 h in total above baseline levels. This time course of recovery and amount of recovery sleep is consistent with experimental studies, and with studies of sleep deprivation using the full Phillips-Robinson model [8]. Furthermore, even after a long deprivation such as this, the simplified model does not enter the unphysical region (iv) discussed in Sec. III D above.

VI. OTHER PHENOMENA

As a brief illustration of the potential fruitfulness of this approach, we now relate the behavior of the model to some phenomena that have been deeply studied in other applications, starting with nonlinear behavior in Sec. VI A, and then stochastic resonance in Sec. VI B.

A. Nonlinear dynamics

The human sleep cycle is typically well entrained to the 24 h light cycle. However, with ageing, the strength of the

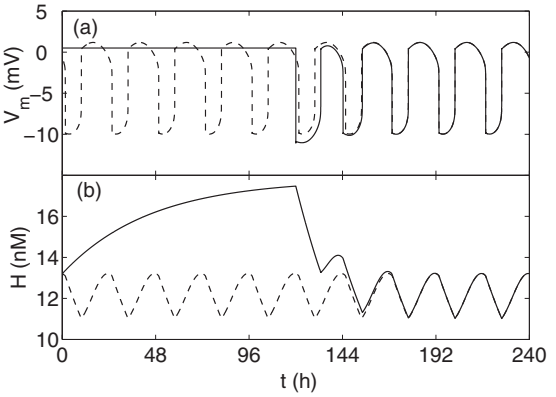

FIG. 11. Simulating a 120 h sleep deprivation protocol followed by recovery (solid line) using the simplified quartic model, as compared to the normal model output (dashed line). Plots are shown for (a) V_m and (b) H.

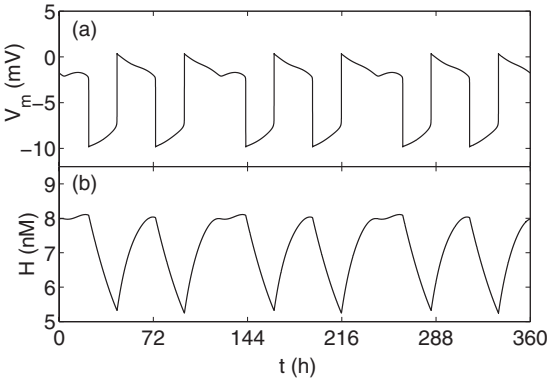

FIG. 12. Model dynamics with $\nu_{vc}=-0.09$ mV and $c_0=70$, with all other parameters nominal. Graphs show (a) V_m and (b) H.

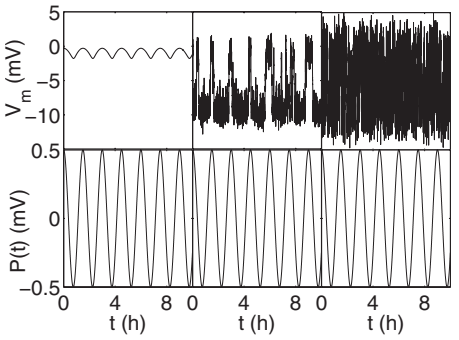

FIG. 13. Plots of V_m versus time with $D=1$ mV and an ultradian signal of amplitude $u_A=0.5$ mV. The first row shows V_m, with noise amplitudes $n_A=0, 0.07, 0.16$ mV running from left to right. The second row shows the ultradian signal $U(t)$ for comparison.

circadian signal relative to the homoestatic drive becomes reduced, due in part to decay of the SCN [14], with a 75% volume loss associated with Alzheimer's disease [15]. This can result in highly fragmented sleep. As an initial demonstration of nonlinear dynamics, we model this by setting $\nu_{vc}=-0.09$ mV, and increasing c_0 to 70 so as to maintain the wake/sleep balance. This disproportionate decrease in ν_{vc} can be justified by the fact that loss of SCN volume can also lead to desynchronization of the oscillator [16]. In this case, we find that the model enters into a 120 h cycle, as shown in Fig. 12, with other periodicities also possible, indicating a possible route into chaotic behavior. Similar dynamics result from significantly increasing ν_{vh} while keeping ν_{vc} constant, and again adjusting c_0 so as to maintain the sleep/wake balance. These results are also achievable in the full model (not shown here), and clearly warrant a systematic investigation of nonlinear dynamics in the model, including bifurcations, period doubling, and a full search of the parameter space for chaotic dynamics.

B. Stochastic resonance

Stochastic resonance occurs in two-well systems when there is a periodic signal present that is of insufficient amplitude to cause state transitions alone, but with the addition of noise, transitions occur in phase with the applied signal [17]. During normal waking, ultradian variations in alertness are observed [18], which are typically insufficient to cause transitions into sleep. Such influences may be sufficient to induce sleep by stochastic resonance in the presence of noise of a suitable amplitude, and this may help to account for phenomena such as daytime napping. Here, we model an ultradian signal by adding a 90 min periodic signal $U(t)=u_A\cos(\phi t)$ to the right-hand side of Eq. (35), with $\phi=2\pi/(1.5)$ h^{-1} and $u_A=0.5$ mV. We fix $D=1$ mV to investigate the effects of this ultradian signal while the model is in a bistable (two-well) state. The behavior of the system for different amplitudes of Gaussian noise is shown in Fig. 13, by also adding the term $n_A\psi(t)$ to the right-hand side of Eq. (35), where values of $\psi(t)$ are drawn randomly from a normal distribution of mean 0 and standard deviation 1, using a timestep of 6 s. For low amplitude noise, the system makes no transitions from wake into sleep. Increasing the amplitude of the noise, the system starts to transition between wake and sleep on an approximately 90 min period, displaying a stochastic resonance. This indicates how even subthreshold stimuli can dictate napping patterns. When the amplitude is increased further, the noise drowns out the ultradian signal, and frequent transitions between states are observed, characteristic of narcolepsy.

VII. DISCUSSION

We have constructed a simplified quartic potential model of the human sleep-wake cycle, by using the potential formulation of a physiologically based model as a starting point. The simplified model was demonstrated to be semiquantitatively consistent with the original model for both normal sleep-wake dynamics and recovery from sleep deprivation, and equally importantly, it is readily fitted to data in its own right. The reduced number of parameters in the simplified model allows for more straightforward and robust fitting and simpler analysis. Furthermore, we gain new insights into the dynamics of the system, in terms of well studied phenomena in mechanical systems, such as friction, stochastic resonance, and nonlinear dynamics. This model does not supersede the physiologically based models, but rather serves a different purpose. This model may thus help able to provide new insights into the dynamics of phenomena that are not yet fully understood at the physiological level, such as the ultradian rhythm.

By formulating the original physiologically based model as a simplified model that simulates the motion of a particle in a one dimensional potential well, we were able to draw on mechanical analogies, and thereby analyze the system from a fresh perspective. The relation described in Sec. III E between friction in the model and the parameters τ_m and τ_v, sheds new light on how these neurotransmitter time constants influence the dynamics. If the value of $\kappa=\tau_m+\tau_v$ is made lower, then the system exhibits underdamped oscillations at the transition between wake and sleep. Furthermore, the model is shown to produce higher order cycles when the strength of the circadian drive is reduced relative to the homeostatic drive, which may lead into chaotic behavior. Such phenomena could foreseeably relate to actual pathologies, in

which case the model may help us to better understand and interrelate their dynamics.

The quartic two-well potential has been studied in a wide variety of applications [19,20], allowing us to make direct relations to phenomena studied in other contexts, thereby gaining a greater insight into the human sleep-wake cycle. For example, the phenomenon of stochastic resonance, in which noise of a suitable amplitude is able to resonantly drive a system between two wells, may be directly related to daytime napping behavior on the time scale of the ultradian rhythm. This may also account for the so-called "forbidden zone," a period of time before the normal sleep onset time during which it is particularly difficult to fall asleep [21]. If ultradian excitation of the MA group is minimal at the time of sleep onset, then we would expect it to be difficult to initiate sleep in the preceding hour when the ultradian excitation would be near its peak. Furthermore, the erratic transitioning seen when the noise amplitude is further increased may relate to narcolepsy. It has been previously shown that decreasing the effect of orexin results in a reduced barrier between wake and sleep states [4], which is equivalent to increasing the noise amplitude with a fixed barrier height. This method therefore also provides a means of estimating the noise amplitude in the physiological system based on the frequency of transitions. In future, the model might also be applied to understanding the statistics of noise-induced sleep/wake transitions, which have been studied experimentally [22].

The simplified quartic model was demonstrated in Sec. V to be readily fitted to data due to its small number of parameters and simple analytic form. In future, such dynamic models may be implemented for fitting to data on an individual basis with greater robustness than models with many free parameters, or previous phenomenological models that have not been directly related to the underlying physiology [23]. Additionally, this model is easily extendable, and provides a platform for future studies of phenomena for which the dynamics are well studied but the underlying physiology is not yet fully understood, such as the ultradian rhythm between REM and NREM sleep. By studying such phenomena in a more compact model of the dynamics, it may enable us to better constrain and infer the underlying physiological structures.

ACKNOWLEDGMENT

The Australian Research Council supported this work.

[1] C. Saper, T. Chou, and T. Scammell, Trends Neurosci. **24**, 726 (2001).
[2] E. Pace-Schott and J. Hobson, Nat. Rev. Neurosci. **3**, 591 (2002).
[3] C. Saper, T. Scammell, and J. Lu, Nature (London) **437**, 1257 (2005).
[4] A. Phillips and P. Robinson, J. Biol. Rhythms **22**, 167 (2007).
[5] Y. Tamakawa, A. Karashima, Y. Koyama, N. Katayama, and M. Nakao, J. Neurophysiol. **95**, 2055 (2006).
[6] C. Diniz Behn, E. Brown, T. Scammell, and N. Kopell, J. Neurophysiol. **97**, 3828 (2007).
[7] M. Carskadon and W. Dement, in *Principles and Practice of Sleep Medicine*, 3rd ed., edited by M. Kyger, T. Roth, and W. Dement (Saunders, Philadelphia, 2000), Chap. 2, pp. 15–25.
[8] A. Phillips and P. Robinson, J. Theor. Biol. **255**, 413 (2008).
[9] C. Czeisler and S. Khalsa, in *Principles and Practice of Sleep Medicine* (Ref. [7]), Chap. 28, pp. 353–375.
[10] A. Borbély and P. Achermann, in *Principles and Practice of Sleep Medicine* (Ref. [7]) (Saunders, Philadelphia, 2000), Chap. 29, pp. 377–390.
[11] H. Goldstein, *Classical Mechanics*, 2d ed. (Addison-Wesley, Reading, 1980).
[12] M. Díaz-Muńoz *et al.*, Sleep Res. Online **2**, 33 (1999).
[13] P. A. Robinson, C. J. Rennie, and J. J. Wright, Phys. Rev. E **56**, 826 (1997).
[14] D. Bliwise, in *Principles and Practice of Sleep Medicine* (Ref. [7]), Chap. 3, pp. 26–42.
[15] D. Swaab, E. Fliers, and T. Partiman, Brain Res. **342**, 37 (1985).
[16] M. Harrington and R. Mistlberger, in *Principles and Practice of Sleep Medicine* (Ref. [7]), Chap. 26, pp. 334–345.
[17] M. McDonnell, N. Stocks, C. Pearce, and D. Abbott, *Stochastic Resonance* (Cambridge University Press, Cambridge, UK, 2008).
[18] N. Kleitman, Sleep **5**, 311 (1982).
[19] L. E. Reichl and W. M. Zheng, Phys. Rev. A **29**, 2186 (1984).
[20] Y. Kim, M. Grabowecky, and S. Suzuki, Vision Res. **46**, 392 (2006).
[21] P. Lavie and A. Scherson, Electroencephalogr. Clin. Neurophysiol. **52**, 163 (1981).
[22] C. Lo, L. Amaral, T. Penzel, P. Ivanov, J. Peter, and H. Stanley, Europhys. Lett. **57**, 625 (2002).
[23] M. Mallis, S. Mejdal, T. Nguyen, and D. Dinges, Aviat Space Environ. Med. **75**, A4 (2004).